RESEARCH ARTICLE

Economic and social modulations of innate decision-making in mice exposed to visual threats

Zhe Li[1,2,3], Jiahui Wang[3], Yidan Sun[3], Jialin Li[3], Ling-yun Li[4], Ya-tang Li[2,3]*

[1]Academy for Advanced Interdisciplinary Studies, Peking University, Beijing, China; [2]Beijing Institute for Brain Research, Chinese Academy of Medical Sciences and Peking Union Medical College, Beijing, China; [3]Chinese Institute for Brain Research, Beijing, China; [4]Department of Neurobiology, School of Basic Medical Sciences, Capital Medical University, Beijing, China

eLife Assessment

The authors show that innate defensive behavior in mice is shaped by threat intensity, reward value, and social hierarchy, highlighting how value and social context influence instinctive decisions. The authors provide a **valuable** characterization of escape behavior which approximates naturalistic conditions. Despite minor methodological limitations, the work provides a **solid** foundation for future investigation of how reward and social context interact to influence behavior.

***For correspondence:** yatangli@cibr.ac.cn

Competing interest: The authors declare that no competing interests exist.

Funding: See page 19

Preprint posted
15 May 2025
Sent for Review
12 May 2025
Reviewed preprint v1
28 July 2025
Reviewed preprint v2
16 March 2026
Reviewed preprint v3
01 July 2026
Reviewed preprint v4
05 August 2026
Version of Record
18 August 2026

Reviewing Editor: Alicia Izquierdo, University of California, Los Angeles, United States

© Copyright Li *et al*. This article is distributed under the terms of the Creative Commons Attribution License, which permits unrestricted use and redistribution provided that the original author and source are credited.

Abstract When confronted by predators, animals make innate decisions with rapid reaction times—a trait shaped by natural selection to maximize survival. However, rapid reactions are effective only when grounded in accurate judgments and appropriate choices, which often require cognitive control. To address how such choices are shaped, we developed a behavioral paradigm to investigate how threat intensity, reward value, and social hierarchy influence decision-making in foraging mice exposed to overhead visual threats. Using a machine learning-based approach, we classified defensive responses into four distinct decision types. Mice showed rapid habituation to repeated looming threats, with substantial inter-individual variability in the rate of habituation. Across both early and late phases of habituation, threat intensity emerged as the primary determinant of decision-making, strongly biasing behavior toward escape. In contrast, the influence of reward value was context-dependent and became evident primarily in the late phase: under low-threat conditions, higher reward value suppressed defensive responses, consistent with value-based decision theory; whereas under high-threat conditions, higher reward value promoted escape, potentially reflecting heightened vigilance. Innate decision-making was further modulated by social hierarchy, with dominant mice showing greater vigilance and a stronger bias toward risk-averse behaviors, while subordinates were more reward-driven. To understand the underlying decision-making process, we developed a drift-diffusion leaky integrator model that successfully captures how threat intensity, reward value, and vigilance interact to shape defensive decisions. Together, these findings reveal how economic and social factors modulate innate decisions and provide a computational framework for understanding the interplay between instinctive reactions and cognitive control.

Introduction

How animals make decisions among alternative actions is a key question in neuroscience. In natural environments, decisions arise from the integration of sensory inputs, internal states, and learned experience (***Meister, 2022***). In the laboratory, both learned and innate paradigms have been used

to study decision-making. Some learned paradigms, such as two-alternative forced choice and Go/No-go tasks (**Burgess et al., 2017**; **Andermann et al., 2010**), often require weeks of training in head-fixed animals; whereas other learned paradigms require less training over several days in freely moving animals, including maze exploration (**Small, 1901**; **Barnes, 1979**; **Morris, 1984**; **Rosenberg et al., 2021**), foraging decisions (**Hayden et al., 2011**; **Steiner and Redish, 2014**; **Hayden, 2018**), and active avoidance (**Mowrer and Lamoreaux, 1946**; **Bravo-Rivera et al., 2014**; **Moscarello and LeDoux, 2013**). While these paradigms have significantly advanced our understanding of the neural mechanisms underlying learned decisions, the training itself may engage neural circuits that differ from those evolved for innate decision-making (**Steinmetz et al., 2019**).

In contrast, innate decisions—such as whether to escape from an approaching aerial predator (**Yilmaz and Meister, 2013**; **De Franceschi et al., 2016**) or a simulated ground threat like a robogator (**Choi and Kim, 2010**; **Amir et al., 2015**)—are executed without prior training and may more directly reflect the function of neural circuits shaped by natural selection. In complex environments, making correct and rapid innate defensive decisions often requires cognitive control to assess risk and evaluate alternative defensive strategies (**Evans et al., 2019**). Defensive responses to terrestrial predators depend on predator–prey distance (**Ydenberg and Dill, 1986**) and are well described by the predatory imminence continuum theory (**Fanselow and Lester, 1988**). Responses to approaching aerial predators are likely scaled similarly according to the perceived threat intensity, which is influenced by the physical properties of the threat (**Yilmaz and Meister, 2013**; **De Franceschi et al., 2016**; **Yang et al., 2020**; **Tammero and Dickinson, 2002**; **Liden and Herberholz, 2008**), prior experience (**Vale et al., 2017**), and environmental context, including housing conditions (**Lenzi et al., 2022**). At the neural level, the superior colliculus (SC) serves as a central hub for processing looming-evoked defensive responses, with distinct output pathways mediating escape versus freezing behaviors (**Evans et al., 2018**; **Shang et al., 2018**; **Zhou et al., 2019**; **Wei et al., 2015**).

Despite this progress, important gaps remain. Mice are social animals, and most predator encounters occur during foraging, yet it is unclear how they weigh perceived threat and reward when making defensive decisions, or how these decisions are influenced by social hierarchy. To address these questions, we developed an ecologically relevant behavioral paradigm to investigate decision-making in foraging mice exposed to overhead visual threats. Our results demonstrate that defensive choices are jointly influenced by threat intensity, reward value, and social hierarchy. Furthermore, we identify vigilance as a key factor linking threat and reward information to behavioral choice. These findings establish a behavioral framework for future investigations into the neural mechanisms underlying the cognitive control of innate decision-making.

Results

A behavioral paradigm for studying innate decision-making in mice

To investigate how animals make innate decisions in natural environments, we designed a behavioral paradigm to simulate the defensive behavior of foraging mice in the wild. In this paradigm, a group of two to five co-housed mice was placed in a nest, with each individual identified using a radio frequency identification (RFID) tag. Only one mouse was allowed to enter a linear arena to receive the reward delivered at the end. As the mouse approached the reward, an overhead expanding dark disc that mimics the approach of an aerial predator was triggered (**Figure 1A**), forcing the animal to decide whether to risk getting the reward or to seek safety in the nest. Behavioral data were recorded using a ground-mounted camera, and DeepLabCut was used to track the movements of the mouse's nose and tail base (**Mathis et al., 2018**; **Figure 1—figure supplement 1A**). Compared with the exploratory phase, looming stimuli significantly increased the frequency of arena entries but decreased the duration of each visit (**Figure 1B, C**).

To identify distinct behavioral patterns in response to looming stimuli, we defined 19 behavioral features from key points of the mouse and fed them into a random forest classifier, which achieved 95% classification accuracy (**Figure 1**, **Figure 1—figure supplement 1B, C**, see Materials and methods). Across 3862 trials, decisions were categorized into four types: direct escape (11.8%, **Video 1**), escape after assessment (assessment + escape, 43.2%, **Video 2**), freezing (5.8%, **Video 3**), and no response (39.2%, **Video 4**; **Figure 1E, F**). A key distinction between assessment + escape and freezing decisions was the duration of stationary behavior: mice that decided to freeze remained stationary significantly

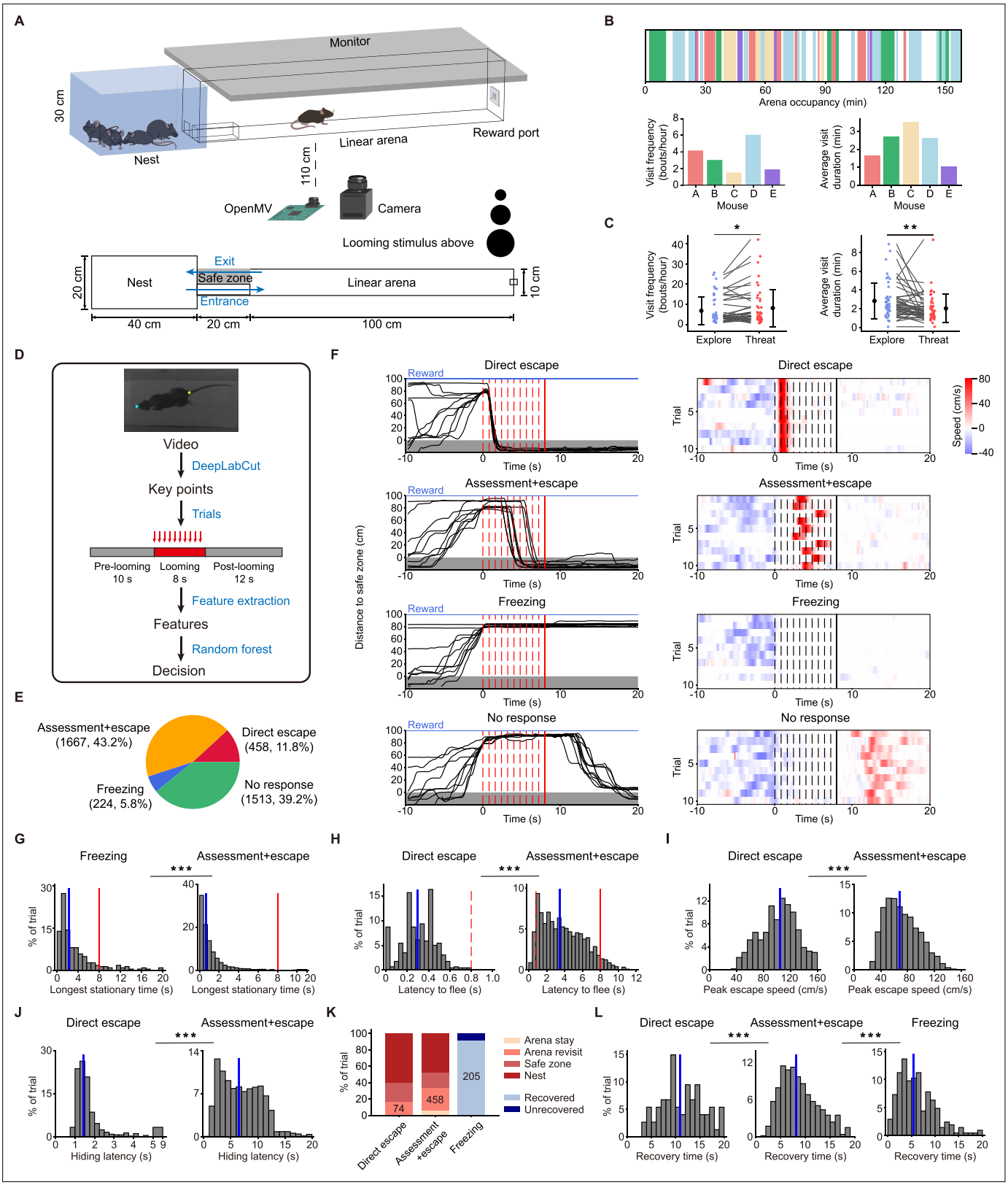


Figure 1. A behavioral paradigm for investigating innate decision-making in mice. (**A**) Schematic of the behavioral assay (3D and top-down views). (**B**) Top: arena occupancy patterns for five example mice in one session. Bottom: visit frequency and average duration for each visit. Different colors mark the mouse's identity. (**C**) Visit frequency and duration under exploration and threat conditions. Error bars represent standard deviation. n = 46 mice; paired t-test. (**D**) Pipeline for behavioral classification. (**E**) Distribution of decisions across 3862 trials from 140 mice. (**F**) Left: distance to the safe zone

Figure 1 continued on next page

Figure 1 continued

over time for four decision types (10 example trials each). Red dashed lines mark the onset of each stimulus repetition; solid lines mark the end of the last repetition. Gray shading indicates the safe zone. Right: locomotion speed toward the safe zone over time for the same trials. Positive speed indicates movement toward the safe zone. (**G**) Distribution of the longest stationary time for 'freezing' and 'assessment + escape'. *n* = 224 and 1667 trials, Mann–Whitney U test. Blue lines mark the median; red solid lines mark the end of the last repetition. (**H**) Distribution of latency to flee for 'direct escape' and 'assessment + escape'. *n* = 458 and 1667 trials, Mann–Whitney U test. Blue lines mark the median; red dashed and solid lines mark the end of the first and last repetitions, respectively. (**I**) Distribution of peak speed for 'direct escape' and 'assessment + escape'. *n* = 458 and 1667 trials, Mann–Whitney U test. (**J**) Distribution of hiding latency in the safe zone for 'direct escape' and 'assessment + escape'. *n* = 455 and 1563, Mann–Whitney U test. (**K**) Distribution of post-decision behavioral states. Numbers indicate the trial counts in which mice recovered from the fear state within 20 s after stimulus onset. (**L**) Distribution of fear recovery time for 'direct escape', 'assessment + escape', and 'freezing'. *n* = 74, 458, and 205, Kruskal–Wallis test followed by Dunn's post hoc test with Holm correction. For all panels: *p < 0.05, **p < 0.01, ***p < 0.001.

The online version of this article includes the following figure supplement(s) for figure 1:

Figure supplement 1. Model validation and feature analysis for automated behavioral classification.

Figure supplement 2. Effects of threat position, prey–threat distance, and prey–safety distance on defensive responses to looming stimuli.

longer than those in the assessment + escape group (***Figure 1G***). In addition, the latency to flee differed significantly between direct escape and assessment + escape decisions (***Figure 1H***).

We hypothesized that fear level increases progressively from freezing to assessment + escape to direct escape. Supporting this hypothesis, mice in the direct escape group exhibited higher escape speeds (***Figure 1I***) and shorter hiding latencies (***Figure 1J***). Moreover, the proportion of mice that recovered within 20 s after stimulus onset was about 16.2%, 27.5%, and 91.5% for direct escape, assessment + escape, and freezing, respectively (***Figure 1K***). Consistently, recovery time decreased progressively across these decision types (***Figure 1L***). These findings align with the predatory imminence continuum theory (***Fanselow and Lester, 1988***), which proposes that defensive responses become more intense as the perceived threat intensity increases.

Mice make economic decisions modulated by vigilance

In the wild, most prey–predator encounters occur during foraging, and prey have evolved to maintain high vigilance to enhance survival. Yet how food value, threat intensity, and vigilance interact to shape defensive decisions remains unclear. To address this question, we developed a behavioral assay that simulates how a foraging animal responds to an approaching aerial predator under different threat and reward conditions (***Figure 2A***). To maintain a consistent internal state across conditions, mice were not water-deprived. The higher reward value of sucrose over water was validated by measuring consumption during exploration (***Figure 2—figure supplement 1A***).

During the first trial, mice showed distinct trajectories and speed profiles across threat and reward conditions (***Figure 2B, C***). These patterns changed rapidly within the first 10 trials, indicating fast habituation to the looming stimulus. This learning was reflected in altered decision patterns (***Figure 2D***) and changes in escape distance, time spent in the reward zone, peak escape speed, and latency to flee (***Figure 2E–H***). To account for both learning and individual variability, we segmented trials for each mouse into early and late phases using a change-point detection approach on the learning curves (***Figure 2I***, ***Figure 2—figure supplement 1C, D***, see Materials and methods).

In the early phase, behavior was shaped predominantly by the level of threat. Under higher threat, mice were more likely to choose direct escape (***Figure 3A***), with longer escape distances (***Figure 3B***) and less time spent in the reward zone (***Figure 3C***), suggesting a trade-off between threat avoidance and reward pursuit. Notably, latency to flee decreased with higher threat (***Figure 3D***), consistent with heightened vigilance (***Buck, 1966***). This threat-dependent change in vigilance was further supported by the longer interval before re-entering the trigger zone and slower foraging speed (***Figure 3E, F***, ***Figure 3—figure supplement 1***), consistent with findings in birds showing that elevated predation risk increases vigilance and reduces feeding time (***Caraco et al., 1980***). In addition, escape speed



Video 1. Example video of a direct escape in response to looming stimuli.
https://elifesciences.org/articles/107306/figures#video1



Video 2. Example video of an escape after assessment decision in response to looming stimuli.
https://elifesciences.org/articles/107306/figures#video2



Video 3. Example video of a freezing decision in response to looming stimuli.
https://elifesciences.org/articles/107306/figures#video3

increased significantly with threat (***Figure 3G***), reflecting the combined effects of perceived higher risk and heightened vigilance. Analyses restricted to the first trial yielded consistent results (***Figure 3—figure supplement 2***).

In the late phase, both threat intensity and reward value contributed to behavior. Threat remained a dominant factor, whereas reward exerted a significant, context-dependent influence. Under low-threat conditions, decisions were primarily driven by perceived reward value. As reward value increased, mice exhibited fewer defensive responses (***Figure 3H***), indicating that they weighed threat and reward to make economic decisions. Higher reward values led to shorter escape distances (***Figure 3I***) and longer stays in the reward zone (***Figure 3J***), supporting value-based decision-making strategies. In contrast, vigilance-related metrics, including latency to flee, foraging interval, and foraging speed, were largely unchanged across reward conditions (***Figure 3K–M***), suggesting that vigilance remained relatively stable. Consistently, escape speed decreased as reward value increased (***Figure 3N***). The value-based decision-making observed under low-threat conditions was further validated using within-subject comparisons to control for individual variability (***Figure 3—figure supplement 3***).

Under high-threat conditions, however, increasing reward value produced the opposite effect: mice showed more direct escape behaviors (***Figure 3H***). This shift in decision patterns was accompanied by behavioral signatures of heightened vigilance, including shorter latencies to flee, longer foraging intervals, and slower foraging speeds (***Figure 3K–M***). These results point to a counterintuitive mechanism: under high threat, reward value does not directly promote continued foraging but instead shapes decisions by enhancing vigilance, which in turn biases animals toward rapid escape responses. Consistent with this interpretation, time spent in the reward zone did not increase with reward value (***Figure 3J***). Collectively, these findings reveal how innate decision-making in response to looming stimuli is shaped by the dynamic interplay between perceived threat intensity and reward value, with vigilance acting as a key modulating factor.

Influence of social hierarchy on decision-making under threat

Mice are social animals that live in groups, where social hierarchy often plays a critical role in shaping behavior. To investigate how social rank influences decision-making under threat, we compared the responses of dominant and subordinate mice to looming stimuli. Rank within each mouse pair was determined using the tube test before and after the behavioral experiments (***Figure 4A***, see Materials and methods), and only pairs with consistent rankings were included in the analysis.

We first verified that behavioral responses to the visual threat were not confounded by the presence of a social partner. Before looming exposure, subordinate mice spent more time exploring the arena than dominant mice (***Figure 4B, C***), which may reflect social avoidance. However, this difference disappeared during and after looming exposure, suggesting that the looming stimulus became the primary driver of behavior. To confirm this, we examined the probability of mice fleeing directly to the nest. If subordinates were avoiding dominants, they would preferentially escape to the safe zone rather than return to the nest occupied by the dominant mouse. Contrary to this prediction, dominant and subordinate mice showed similar probabilities of fleeing directly to the nest (***Figure 4D***), indicating that defensive responses were driven primarily by the visual threat rather than social avoidance.

When threat and reward co-localized, only dominant mice reduced their relative time spent in the reward zone during the 2-hr session (***Figure 4E, F***), indicating greater vigilance and risk aversion than subordinate mice. This heightened vigilance in dominant mice was further supported by reduced habituation to the looming threat (***Figure 4G, H***, ***Figure 4—figure supplement 1***), a higher proportion of direct escape decisions (***Figure 4I***), and shorter latencies to flee (***Figure 4J***). No rank differences were observed in foraging intervals or foraging speeds (***Figure 4K, L***). This may stem from the experimental design, in which only one mouse was allowed in the arena at a time, potentially limiting the sensitivity of these measures to detect rank-dependent differences in vigilance.



Video 4. Example video of a no response decision in response to looming stimuli.
https://elifesciences.org/articles/107306/figures#video4

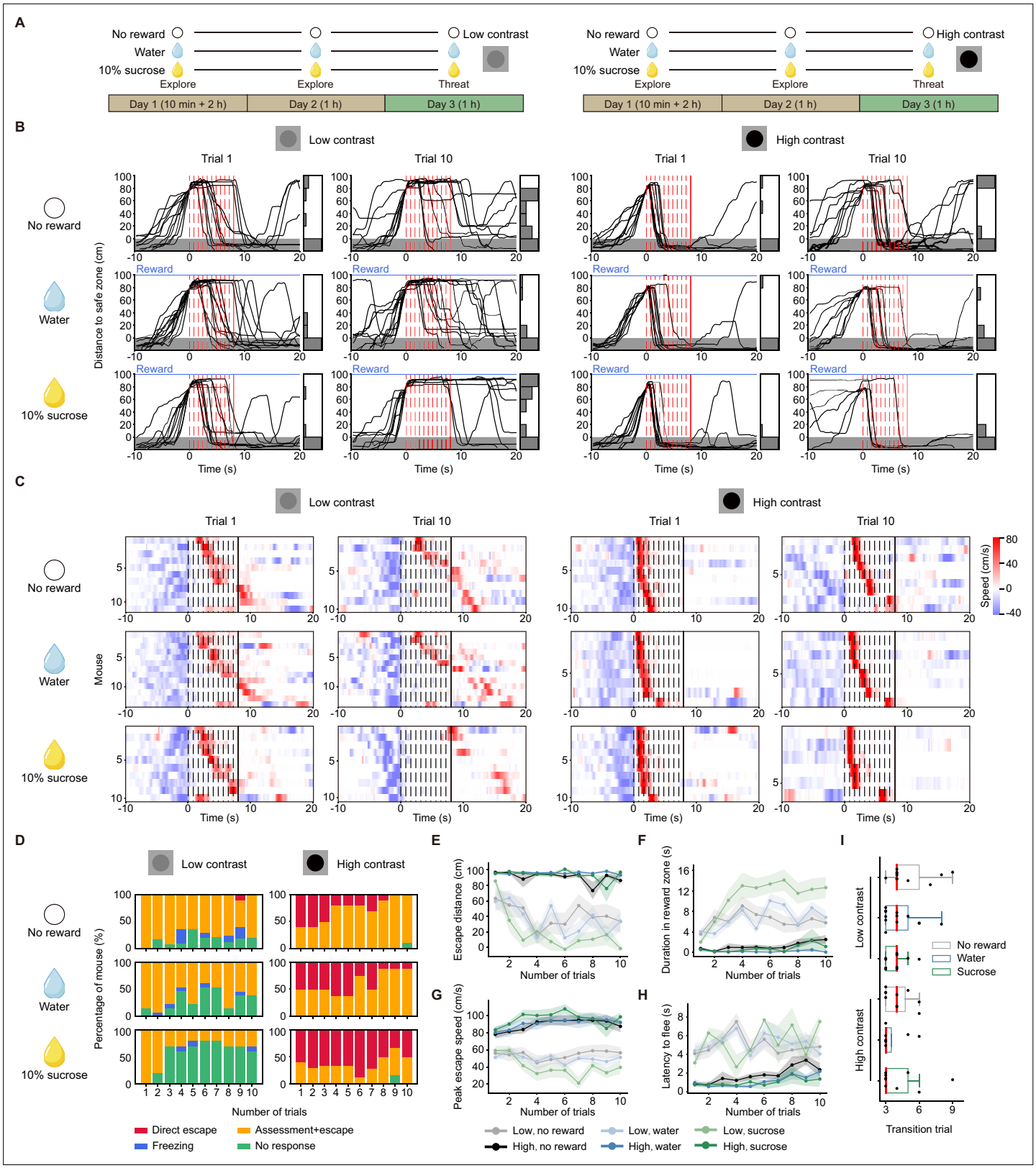


Figure 2. Rapid learning shapes economic decisions under threat. (**A**) Schematic of the behavioral assay for studying the economic modulation of innate decision-making. (**B, C**) Distance to the safe zone and locomotion speed over time for the first and tenth trials in response to low- and high-contrast looming stimuli across different reward conditions. The right inset in (**B**) shows the distribution of distance to the safe zone at the end of each trial. Dashed lines mark the start of each stimulus, and solid lines mark the stimulus offset. *n* = 11 (no reward, low), 13 (water, low), 10 (sucrose, low), 10

Figure 2 continued on next page

Figure 2 continued

(no reward, high), 8 (water, high), and 10 (sucrose, high) mice. (**D**) Summary of the decisions across the first 10 trials under different threat and reward conditions. *n* = 11, 13, 10, 10, 8, and 10 mice. (**E–H**) Escape distance under threat, duration in the reward zone, peak escape speed, and latency to flee across trials in all conditions. Shading denotes the standard error of the mean. (**I**) Transition trials marking the shift between phases across conditions. Red lines indicate the median; boxes span the interquartile range (IQR); whiskers extend to 1.5 × IQR beyond the box.

The online version of this article includes the following figure supplement(s) for figure 2:

Figure supplement 1. Control analyses of consummatory behavior, looming detection, and behavioral dimensionality.

Furthermore, dominant mice prioritized threat avoidance over reward, fleeing longer distances at higher escape speeds and spending less time in the reward zone (***Figure 4M–O***). To rule out the possibility that the tube test itself influenced defensive behavior, we conducted additional experiments in which looming sessions occurred both before and after the tube test (***Figure 4—figure supplement 2***); the results remained largely consistent. Together, these findings indicate that social hierarchy biases the trade-off between reward seeking and threat avoidance, with dominant mice exhibiting heightened threat vigilance and subordinate mice showing stronger reward-driven behavior.

A mathematical model for innate decision-making under threat

Our experimental results demonstrate that innate decision-making in response to visual threats is influenced by perceived threat intensity, reward value, and vigilance. To understand the underlying decision-making process, we developed a mathematical model in which evidence for escape is accumulated by a drift-diffusion leaky integrator. An escape response is triggered when the evidence level crosses a predefined threshold:

$$\mathrm{d}x_i(t) = (-\alpha x_i(t) + \beta s(t) - r)\mathrm{d}t + \delta \mathrm{d}W(t), \tag{1}$$

$$E(t) = \mathcal{H}\left(x_i(t) - x_{\mathrm{thr}}\right). \tag{2}$$

Here, $x_i(t)$ is the accumulated escape evidence at time t on the ith trial. The leakage rate α drives the evidence toward zero and is equal to the reciprocal of the integration time constant. The stimulus function $s(t)$ denotes the normalized diameter of the looming stimulus (***Figure 5—figure supplement 1A***). Together with the threat gain β, which reflects both stimulus contrast and the animal's vigilance level, these terms determine the perceived threat intensity and drive evidence accumulation toward escape. The term r represents the perceived reward valueand suppresses the accumulation of escape evidence. The stochastic term $\mathrm{d}W(t)$ denotes increments of a Wiener process, satisfying $W(t+\Delta t) - W(t) \sim \mathcal{N}(0, \Delta t)$, and δ is the diffusion rate. The binary variable $E(t)$ indicates whether an escape decision has been reached, with $\mathcal{H}$ denoting the Heaviside step function and x_{thr} the decision threshold. If a decision is reached within the first expansion of the looming disc, it is classified as a direct escape; otherwise, it is classified as an escape after assessment.

Model parameters were estimated using behavioral data from the late phase of the reward–threat experiments in two steps (see Materials and methods). First, we fit the model to data under the no-reward condition to obtain the optimal leakage rate ($\alpha = 1.78$), threat gain (low threat: $\beta = 1$; high threat: $\beta = 1.44$), diffusion rate ($\delta = 5.6$), and decision threshold ($x_{\mathrm{thr}} = 0.71$) (***Figure 5—figure supplement 1B***). These parameters reveal distinct decision-making dynamics under low- and high-threat conditions. Under low threat, the average evidence level remains below the escape threshold, and escape decisions emerge from stochastic fluctuations in individual trials (***Figure 5A***). Under high threat, the average evidence level crosses the threshold, indicating that escape decisions are mainly driven by threat gain (***Figure 5B***). Notably, threat gain and diffusion rate exert distinct effects on latency to flee: threat gain shifts the mean latency, while diffusion rate affects its variance. Thus, the model captures not only the observed decision patterns but also the distributions of latency to flee.

Second, we identified threat gain and reward value across threat and reward conditions in the late phase (***Figure 5—figure supplement 1C, D***). Consistent with experimental findings that decisions under low threat are primarily driven by reward value, the fitted reward-value parameter increases across reward conditions (0, 0.08, and 0.25 for no reward, water, and sucrose, respectively). With these parameters, the model reproduces the observed reduction in escape likelihood without changes in latency to flee (***Figure 5A, C, E***). The same reward-value parameters were then used to model the decision-making process under high-threat conditions. Here, the fitted threat-gain parameter increases

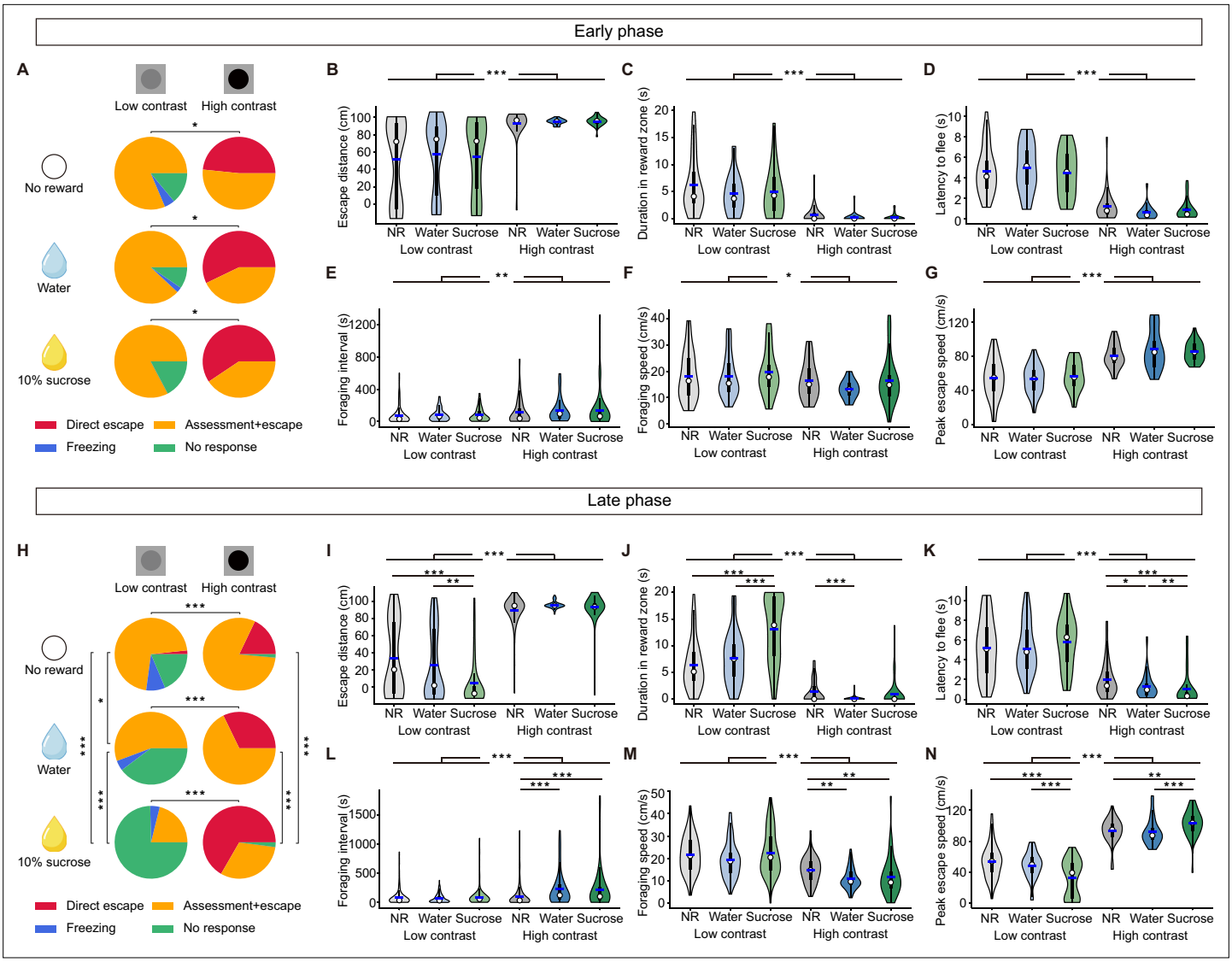


Figure 3. Mice make economic decisions modulated by vigilance. (**A**) Distribution of decisions in the early phase under six experimental conditions. *n* = 43 trials from 11 mice (no reward, low), 42 trials from 13 mice (water, low), 29 trials from 10 mice (sucrose, low), 31 trials from 10 mice (no reward, high), 21 trials from 8 mice (water, high), and 32 trials from 10 mice (sucrose, high); chi-squared test. (**B–G**) Escape distance under threat, duration in the reward zone, latency to flee, foraging interval, foraging speed, and peak escape speed in the early phase across all conditions. *n* = 43, 42, 29, 31, 21, and 32 trials for **B, C, F, G**; *n* = 35, 37, 24, 31, 21, and 32 trials for **D**; *n* = 116, 84, 54, 58, 36, and 48 intervals for **E**; Scheirer–Ray–Hare test with post hoc Dunn's test (Holm correction). (**H**) Distribution of decisions in the late phase under six experimental conditions. *n* = 59 trials from 11 mice (no reward, low), 88 trials from 13 mice (water, low), 71 trials from 10 mice (sucrose, low), 67 trials from 10 mice (no reward, high), 59 trials from 8 mice (water, high), and 48 trials from 9 mice (sucrose, high); chi-squared test. (**I–N**) Escape distance under threat, duration in the reward zone, latency to flee, foraging interval, foraging speed, and peak escape speed in the late phase across all conditions. *n* = 59, 88, 71, 67, 59, and 48 trials for **I, J, M, N**; *n* = 43, 49, 15, 66, 59, and 47 trials for **K**; *n* = 116, 182, 114, 137, 71, and 57 intervals for **L**; Scheirer–Ray–Hare test with post hoc Dunn's test (Holm correction). For all panels: *p < 0.05, **p < 0.01, ***p < 0.001.

The online version of this article includes the following figure supplement(s) for figure 3:

Figure supplement 1. Distribution of foraging speed.

Figure supplement 2. Behavioral responses to looming stimuli across threat and reward conditions in the first trial.

Figure supplement 3. Reward modulation of defensive behavior to looming stimuli within the same mouse.

across reward conditions (1.44, 1.8, and 2.55 for no reward, water, and sucrose, respectively), counteracting—and ultimately reversing—the influence of reward value. The model again reproduces the experimentally observed increase in escape decisions and decrease in latency to flee (***Figure 5B, D, F***).

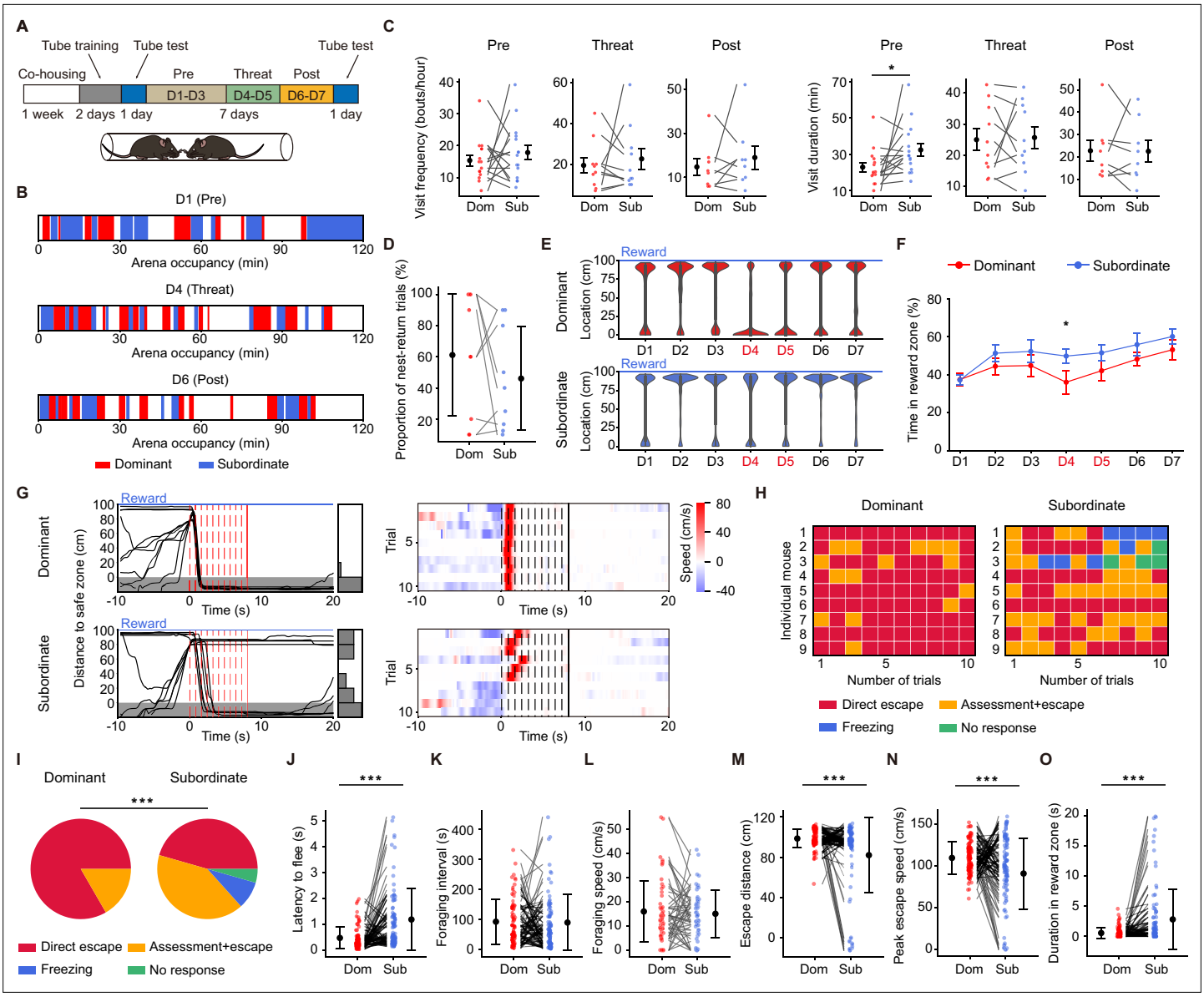


Figure 4. Influence of social hierarchy on innate decision-making. (**A**) Schematic of the behavioral assay for studying the social modulation of innate decision-making. Top, experimental timeline. Each session lasted 2 hr per mouse pair during the pre-threat, threat, and post-threat phases. Bottom, schematic of the tube test. (**B**) Arena occupancy for an example pair of mice during the three sessions. (**C**) Visit frequency and total visit duration for dominant and subordinate mice during the pre-threat, threat, and post-threat sessions. n = 5 pairs (pre), 5 pairs (threat), and 4 pairs (post), respectively; paired t-test. (**D**) Proportion of nest-return trials in escape trials for dominant and subordinate mice. n = 9 pairs; paired t-test. (**E**) Distance to the safe zone over 7 days for an example pair. Looming stimuli were presented on days 4 and 5. (**F**) Percentage of time spent in the reward zone across days. Error bars represent SEM. n = 9 pairs; paired t-test. (**G**) Distance to the safe zone (left) and locomotion speed (right) for an example pair. (**H**) Behavioral decisions across the first 10 trials for 9 mouse pairs. (**I**) Pie charts showing decision distributions for dominant and subordinate mice. n = 90, 90 trials; Stuart–Maxwell test. (**J–O**) Latency to flee, foraging interval, foraging speed, escape distance under threat, peak escape speed, and duration in the reward zone for dominant and subordinate mice. n = 78 trials for **J**; n = 75 trials for **K**, 53 for **L**, and 90 for **M–O**; paired t-test. For all panels: *p < 0.05, **p < 0.01, ***p < 0.001.

The online version of this article includes the following figure supplement(s) for figure 4:

Figure supplement 1. Behavioral responses to looming stimuli for dominant and subordinate mice in different phases.

Figure supplement 2. Comparison of behavioral responses to looming stimuli before and after the tube test.

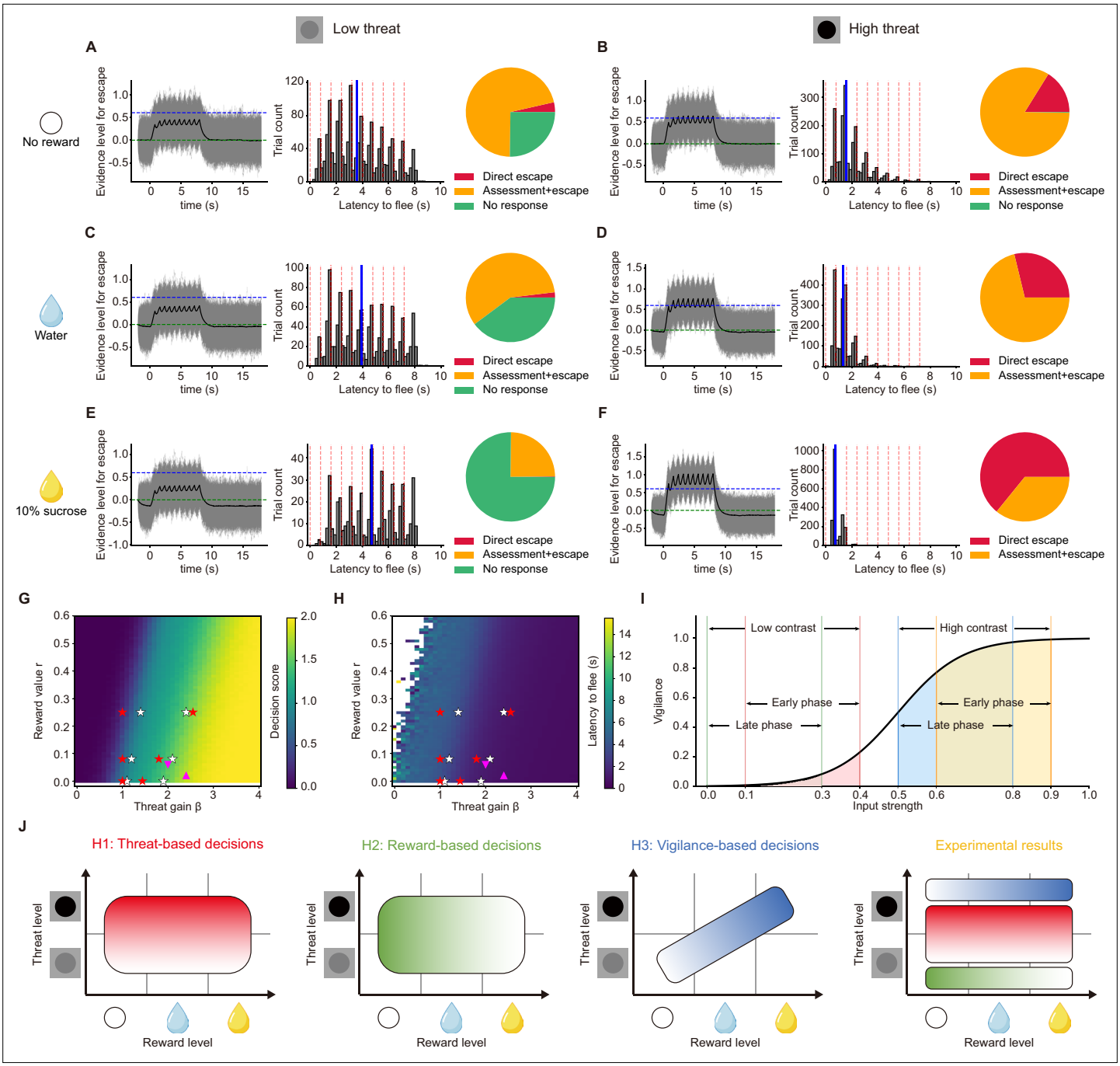


Figure 5. Drift-diffusion leaky integrator model for escape decisions. (**A–F**) Simulated accumulation of escape evidence, along with predicted latencies to flee and decision distributions across six threat and reward conditions. Green dashed horizontal lines mark $x = 0$; blue dashed horizontal lines mark $x = x_{\text{thr}}$; red dashed vertical lines mark the onset of each looming stimulus; blue vertical lines mark the median. (**G**) Heatmap of decision scores as a function of threat gain and reward value. White and red stars indicate fitted parameters for the early and late phases of the reward–threat paradigm, respectively; upward and downward pink triangles indicate fitted parameters for dominant and subordinate mice in the social-threat paradigm, respectively. (**H**) Heatmap of latencies to flee as a function of threat gain and reward value. (**I**) Vigilance as a function of input strength, illustrating how the indirect effect of reward on defensive decisions via vigilance depends on the baseline vigilance level. (**J**) Schematic showing how threat intensity, reward value, and vigilance jointly determine defensive decisions. Color saturation indicates defense likelihood.

The online version of this article includes the following figure supplement(s) for figure 5:

Figure supplement 1. Fitting loss in the drift-diffusion leaky integrator model.

To assess the model's predictive power, we simulated how decision score (see Materials and methods) and latency to flee vary as functions of reward value (r) and threat gain (β). Increasing reward generally reduces decision score and increases latency to flee, whereas increasing threat gain has the opposite effect (***Figures 5G, H*** and ***Figure 5—figure supplement 1E–G***). These relationships are confirmed by a simplified deterministic model (***Figure 5—figure supplement 1H–K***, see Materials and methods). Notably, reward can also indirectly promote escape via elevated vigilance, and the magnitude of this effect depends on the level of baseline vigilance, defined as vigilance in the absence of reward (***Figure 5I***). This dual influence explains the absence of a reward effect in the early phase under both threat conditions: high vigilance shifts the operating range to a region where reward's indirect promoting effect is balanced by its direct suppressing effect on escape decisions.

We next applied this model to the social-threat paradigm. The behavior of dominant mice is captured by a combination of lower reward value and higher threat gain compared to subordinates (pink triangles in ***Figure 5G, H***). This aligns with the experimental finding that dominant animals spent less time in the reward zone and fled more quickly (***Figure 4J, O***). Together, these results demonstrate that the model robustly captures key behavioral features across phases and paradigms, providing a unified mechanistic account of innate decision-making under threat (***Figure 5J***).

Discussion

When confronted by a predator, an animal must rapidly decide whether to escape, freeze, or continue its ongoing behavior. This life-or-death decision is especially critical for rodents facing aerial predators. Although mice are social animals and most predator encounters occur during foraging, it remains unclear how they integrate perceived threat and reward when making defensive decisions, or how these decisions are further influenced by social hierarchy. Using a foraging-based paradigm, we demonstrate that responses to visual threat are shaped by threat intensity, reward value, social rank, and internal state, and that this integrated decision process can be captured by a drift-diffusion leaky integrator.

Main findings

We designed a behavioral paradigm to simulate how mice respond to visual threats during foraging (***Figure 1***). Mice adapted rapidly to repeated looming stimuli, showing substantial inter-individual variability in the rate of habituation (***Figure 2***). While threat intensity robustly shaped behavior in both early and late phases of habituation, reward exerted a clear influence only in the late phase (***Figure 3***). Specifically, increasing threat intensity shifted behavior toward more defensive responses. Reward, in contrast, produced a context-dependent effect: under low-threat conditions, higher reward values suppressed defensive responses, consistent with value-based decision theory, whereas under high-threat conditions, they promoted escape decisions, likely through heightened vigilance. Innate decision-making was further shaped by social hierarchy (***Figure 4***): dominant mice exhibited a stronger bias toward defensive behaviors, whereas subordinates were more reward-driven and less likely to flee. Finally, we developed a drift-diffusion leaky integrator model that captures the key features of the observed behavioral patterns, providing a unified framework for understanding how threat, reward, and social context interact to shape innate defensive decisions (***Figure 5***).

Relation to earlier work

Aerial predators pose a significant threat to rodents. Previous studies have shown that overhead visual stimuli in the laboratory elicit robust defensive behaviors in rodents (***Wallace et al., 2013***; ***Yilmaz and Meister, 2013***). Because these stimuli can mimic distinct predatory actions, the resulting behavioral responses depend on the physical properties of the stimulus. For example, an overhead expanding dark disc mimicking an approaching aerial predator preferentially triggers escape rather than freezing (***Yilmaz and Meister, 2013***), while a small black moving dot mimicking a cruising predator predominantly induces freezing behavior (***De Franceschi et al., 2016***). These findings suggest that the response is not a simple reflex but involves a decision-making process. Additional stimulus properties that influence action selection include contrast, speed, size, and shape (***Yang et al., 2020***; ***Evans et al., 2018***; ***De Franceschi et al., 2016***). Further support for a decision-making process comes from its modulation by environmental factors and experience: mice freeze more when no refuge is



Video 5. Example video showing defensive responses to looming stimuli presented behind the mouse.
https://elifesciences.org/articles/107306/figures#video5



Video 6. Example video showing defensive responses at a prey–threat distance of 35 cm.
https://elifesciences.org/articles/107306/figures#video6

available (***Wei et al., 2015***) and quickly learn that the looming stimulus poses no real threat (***Lenzi et al., 2022***; ***Zhong et al., 2023***; ***Vale et al., 2017***). This innate decision-making process is observed across invertebrates and vertebrates (***Evans et al., 2019***).

Methodologically, the present study differs from earlier work in two aspects. First, instead of manually annotating behavioral responses, we employed a machine learning-based approach to classify behavioral decisions. Similar strategies have been used in previous studies of defensive behaviors (***Fratzl et al., 2021***). In our dataset, this approach substantially reduced the labor required for labeling and minimized misclassifications due to inter-individual variability. Second, unlike previous studies using 2D arenas, we designed a linear arena to simulate foraging conditions, in which the nest and reward zone were separated by a long corridor. Decision patterns in this assay closely matched those reported in 2D paradigms (***Yang et al., 2020***), including rapid habituation to looming stimuli over the first few trials (***Lenzi et al., 2022***). However, mice exhibited more frequent escape responses to low-contrast looming stimuli than reported in 2D arenas (***Evans et al., 2018***; ***Fratzl et al., 2021***), suggesting that the linear configuration lowers the escape threshold in response to weak threat cues.

One concern with the linear arena design was that the looming stimulus was usually presented at the end of the arena, raising the possibility that mice simply retreated upon reaching a physical boundary. To address this, we presented the stimulus between the foraging mice and the nest (***Figure 1—figure supplement 2A***). Under this condition, mice rapidly fled toward the nest—and thus toward the threat—rather than away from it (***Figure 1—figure supplement 2B***, ***Video 5***). This behavior indicates that their escape responses are not simple reflexes, but instead incorporate the safety of the nest into their decisions.

Fanselow and Lester's predatory imminence continuum theory posits that defensive behaviors are graded according to perceived threat intensity (***Fanselow and Lester, 1988***). To test whether this framework applies to aerial threats, we varied both prey–threat distance and prey–safety distance. As prey–threat distance increased, mice showed less direct escape behavior, with longer latencies to flee and slower escape speeds (***Figure 1—figure supplement 2C–G***, ***Videos 6–8***), indicating that defensive responses scale with threat proximity. These effects cannot be explained by failure to detect the stimulus at longer distances; if that were the case, foraging speed would remain unaffected. Instead, mice slowed as they approached the threat in the 75 cm condition (***Figure 1—figure supplement 2D***). In contrast, prey–safety distance did not significantly influence defensive behaviors (***Figure 1—figure supplement 2H, I***). One interpretation is that once an aerial threat is detected, the urgency to escape overrides evaluation of refuge proximity. To further verify this, we introduced barriers that lengthened the return path to the nest. Even under these conditions, defensive behaviors remained unaffected by prey–safety distance (***Figure 1—figure supplement 2J, K***, ***Video 9***).

Economic and social modulations of innate decision-making under threat

Value-based decision-making—where choices arise from comparisons of the subjective value of expected outcomes—is a well-established framework for understanding behavior across species (***Rangel et al., 2008***). Prospect theory, which accounts for decision-making under risk in humans (***Kahneman and Tversky, 1979***), has been applied to learned decision-making in rodents (***Constantinople et al.,***



Video 7. Example video showing defensive responses at a prey–threat distance of 55 cm.
https://elifesciences.org/articles/107306/figures#video7



Video 8. Example video showing defensive responses at a prey–threat distance of 75 cm.
https://elifesciences.org/articles/107306/figures#video8



Video 9. Example video showing defensive responses to looming stimuli in the linear arena with barriers.
https://elifesciences.org/articles/107306/figures#video9

2019). Here, we demonstrate that value-based decision-making also extends to innate defensive behaviors: when confronted with a threat, mice integrate perceived reward and threat value to make their decisions.

Importantly, perceived value is determined not only by the physical properties of the stimulus but also by the animal's internal state. In the resting state, for example, perceived stimulus strength scales with physical intensity according to the Weber–Fechner law. In our paradigm, perceived threat value is strongly modulated by vigilance, a state of heightened and sustained attention to potential danger. This vigilance-dependent modulation substantially alters how the same looming stimulus is evaluated and how decisions are made.

Consistent with value-based evaluation, increasing threat intensity reliably increased defensive responses across reward conditions and behavioral phases. These changes reflect differences in perceived threat rather than stimulus detection, as evidenced by coordinated changes in escape latency, distance, and speed, and further supported by trial-by-trial inspection confirming reliable stimulus detection across contrast levels (***Figure 2—figure supplement 1B***).

Reward-dependent behavior also follows value-based principles, but in a vigilance-dependent manner. In nature, foraging often occurs under predation risk, and evolutionary pressure has favored prey that maintain heightened vigilance in the presence of high-value rewards. Consistent with this, more valuable rewards increased both perceived reward value and—via elevated vigilance—perceived threat value. These opposing effects jointly shaped the escape decision.

In the early phase, baseline vigilance is already high because looming represents an innate threat. Under this high-vigilance condition, more valuable reward elevates both perceived reward and threat value; these opposing effects counterbalance each other, resulting in no detectable behavioral differences across reward conditions. With repeated exposure, habituation to looming reduces vigilance, shifting the operating range leftward along a sigmoidal vigilance-intensity function (***Figure 5I***). This sigmoidal form is biologically plausible, as vigilance is bounded by a relaxed-state minimum and by cognitive capacity limits. This shift has opposite consequences under low- versus high-threat conditions. Under low threat in the late phase, reduced vigilance compresses the dynamic range, weakening the indirect effect of reward on perceived threat and allowing perceived reward value to dominate decisions. Under high threat, however, the vigilance function remains within a steeper region of the sigmoid, where increases in reward effectively elevate vigilance and thus perceived threat. As a result, reward produces the opposite behavioral effect under high threat. Together, these dynamics explain why reward effects are absent early but emerge after habituation in a threat-dependent manner.

Social rank-dependent differences in defensive behavior also fit within this framework. Even under identical conditions, dominant mice perceived higher threat values—driven by their elevated vigilance—along with lower reward values, consistent with their more risk-averse behavior. Similar status-dependent escape patterns have been reported across species, including voles (***Kleiman et al., 2014***) and crayfish (***Krasne et al., 1997***), suggesting an evolutionarily conserved strategy.

Because vigilance declines with habituation, factors that modulate the rate of habituation also influence defensive behavior. Although individuals vary, several patterns emerged. Mice habituated more rapidly under high-threat or high-reward conditions (***Figure 2I***). Dominant mice habituated more slowly than subordinates, consistent with their elevated vigilance (***Figure 4H***, ***Figure 4—figure supplement 1A***). Housing conditions also altered habituation: group-housed animals adapted more slowly to looming than single-housed animals, and dominant–subordinate pairs habituated even more slowly than group-housed mice (***Figure 2I***, ***Figure 4—figure supplement 1A***). These patterns indicate that stable social relationships sustain high vigilance and slow habituation—an evolutionarily conserved strategy that may enhance survival. Importantly, vigilance should not be conflated with stress or anxiety-like states. The slower habituation observed in group-housed mice reflects sustained sensitivity to repeated threat exposure rather than elevated anxiety. Thus, our data do not contradict the concept of social buffering; rather, they are consistent with it, as pair-housed mice exhibited reduced defensive responses compared with individually housed animals (***Lenzi et al., 2022***). Furthermore, in an independent study (***Li et al., 2026b***), we observed that mice tested in the presence of a

social partner displayed attenuated responses to looming stimuli relative to those tested alone. These findings suggest that social interactions can attenuate defensive responses while prolonging vigilance during repeated threat exposure.

One limitation of the present study is that our experiments were conducted exclusively in male mice to avoid the confounding effects of behavioral variability associated with the female estrous cycle. Extending this paradigm to females—with careful control for estrous cycle—will provide a more comprehensive understanding of how economic and social factors modulate defensive decision-making.

A proposed role for the SC in value integration

What neural circuits underlie the economic and social modulations of decision-making under threat? A growing body of research implicates the SC as a key node in looming-evoked defensive behaviors (***Wei et al., 2015***; ***Shang et al., 2015***; ***Evans et al., 2018***). In parallel, reward is encoded by dopaminergic neurons in the ventral tegmental area (***Schultz, 1998***; ***Cohen et al., 2012***) and serotonergic neurons in the dorsal raphe nucleus (***Miyazaki et al., 2011***; ***Liu et al., 2014***), which project widely to regions such as the ventral striatum (***Schultz et al., 1992***), orbitofrontal cortex (***Tremblay and Schultz, 2000***), and cerebellum (***Wagner et al., 2017***). Furthermore, social status modulates behavior via circuits involving the medial prefrontal cortex (mPFC) (***Kingsbury et al., 2019***; ***Wang et al., 2011***) and serotonergic signaling (***Edwards and Kravitz, 1997***; ***Yeh et al., 1997***; ***Raleigh et al., 1991***).

We propose the SC as a central integrative hub for mediating the economic and social modulation of defensive decision-making. First, neurons in the superficial (sSC) and intermediate (iSC) layers of the medial SC are critical in detecting looming threats and triggering defensive responses (***Li et al., 2020***; ***Li et al., 2023***; ***Wei et al., 2015***; ***Evans et al., 2018***). Second, two lines of evidence support reward modulation of the SC. On the one hand, neurons in the medial iSC express dopamine and serotonin receptors (***Woolrych et al., 2021***; ***Mooney et al., 1996***), with D1 receptors enriched in the sSC and D2 receptors in the iSC, suggesting that threat signals can be integrated with reward- and social-related information in a layer-dependent manner. Indeed, reward-related signals have been reported in the medial sSC (***Baruchin et al., 2023***). On the other hand, whereas the medial SC preferentially mediates defensive responses, the lateral SC promotes approach behaviors toward rewarding stimuli, such as food or prey (***Krauzlis et al., 2013***; ***Comoli et al., 2012***), suggesting that medial–lateral interactions within the SC may play a critical role in resolving threat–reward trade-offs during decision-making. Third, social modulation can be conveyed through mPFC inputs and serotonergic pathways, providing a route for social status to directly bias SC computations underlying defensive decisions (***Kingsbury et al., 2019***; ***Wang et al., 2011***; ***Edwards and Kravitz, 1997***; ***Yeh et al., 1997***; ***Raleigh et al., 1991***).

Finally, SC computations are further shaped by contextual and experience-dependent signals that jointly influence economic and social modulation of behavior. The medial iSC receives inputs from the retrosplenial cortex and hippocampus (***Campagner et al., 2023***; ***Benavidez et al., 2021***), providing spatial and mnemonic context for evaluating threat and reward contingencies (***Calvin et al., 2025***). Consistently, looming stimuli engage hippocampal CA1 neurons (***Conway et al., 2025***). Moreover, repeated exposure induces habituation and fear extinction through a cortico-subcortical pathway in which higher visual areas recruit inhibitory neurons in the ventral lateral geniculate nucleus to suppress medial iSC activity (***Salay and Huberman, 2021***; ***Fratzl et al., 2021***; ***Mederos et al., 2025***), indicating experience-dependent reweighting of SC-mediated responses. These threat, reward, social, and contextual signals are integrated in the iSC and conveyed to the deep SC, which interfaces with downstream brainstem and midbrain effector systems, including the periaqueductal gray and substantia nigra dopaminergic neurons (***Comoli et al., 2003***), enabling rapid transformation of integrated signals into defensive and approach actions.

While anatomical and functional evidence supports the SC as a central integrative hub, we emphasize that the neural architecture underlying such decisions is far more complex. The precise integration of internal state, social rank, and external threat likely emerges from the dynamic interplay of distributed circuits, including prefrontal, limbic, and neuromodulatory systems. Dissecting how these circuits interact to shape defensive decisions remains an important direction for future research.

Mathematical modeling

The proposed drift-diffusion leaky integrator model builds on an integrator model of internal state (***Gibson et al., 2015***) and extends it by incorporating a reward-driven drift-diffusion process (***Ratcliff, 1978***). Conceptually, the integrator component in our model aligns with Lorenz's 'hydraulic' model of motivation, which describes how internal drives shape behavior (***Lorenz, 1950***). While our model resembles the leaky integrator used to model escape behavior in flies (***Gibson et al., 2015***), it differs in several ways. First, the earlier model lacks a reward-related drift component. Second, while that model treats the looming effect as a delta function, our model allows the evidence level to vary continuously with stimulus size. Third, the influence of vigilance is absent in that model. A similar model has been proposed (***Evans et al., 2018***), but it did not incorporate reward and vigilance. Note that the evidence level for escape in our model is not equivalent to fear level (***Anderson and Adolphs, 2014***); rather, when it crosses a threshold, the animal may enter a fear state.

Below, we briefly discuss the roles of individual parameters. The leakage rate α represents a drive toward the resting state. Perceived threat is modeled as the product of the threat gain β and the sensory input $s(t)$ and promotes escape decisions, whereas perceived reward r drives the decision away from escape. The threat gain increases not only with threat intensity but also with reward value via its influence on vigilance. The effect of reward on vigilance depends on the operating region of the sigmoidal vigilance function. This operating region is set by the baseline vigilance level (***Figure 5I***) and reflects habituation to repeated looming threats. Furthermore, threat gain and reward value have distinct effects on escape latency: higher threat gain exponentially shortens latency, whereas higher reward value increases it linearly (***Figure 5—figure supplement 1F–H***). These effects are confirmed using a simplified deterministic version of the model (***Figure 5—figure supplement 1J, K***, see Materials and methods).

Lastly, the diffusion rate δ plays a critical role, particularly under low-threat conditions where the average evidence trajectory fails to reach the threshold. This parameter may reflect fluctuations of the animal's internal state. The diffusion rate captures the trial-to-trial variability: even small amounts of noise can accumulate over time, resulting in large differences across individual trials and contributing to variability in escape latency. Overall, this computational framework not only accounts for our experimental observations but also offers a quantitative foundation for studying innate decision-making across species. Understanding how these parameters are implemented at the circuit level is an exciting direction for future research.

Materials and methods

Key resources table

Reagent type (species) or resource	Designation	Source or reference	Identifiers	Additional information
Strain, strain background (*M. musculus*, male)	C57BL/6J	Chinese Institute for Brain Research, Beijing	RRID:IMSR_JAX:000664	
Chemical compound, drug	Sucrose	Sigma-Aldrich	Cat#:V900116	
Software, algorithm	Python v3.9	Python Software Foundation	RRID:SCR_008394	
Software, algorithm	R v4.2.1	R Project for Statistical Computing	RRID:SCR_001905	

Animals

Male C57BL/6J mice were group-housed on a 12-hr light/12-hr dark cycle and used at 2–3 months of age. Behavioral experiments were conducted during the light phase. All experimental procedures were performed under the animal welfare guidelines and approved by the Institutional Animal Care and Use Committee at the Chinese Institute for Brain Research, Beijing.

Behavioral platform

The behavioral platform consisted of a nest, a linear arena, a reward-delivery port, and an automated tracking system that included RFID and real-time position detection. As illustrated in ***Figure 1A***, the nest (40 (*L*) × 20 (*W*) × 30 (*H*) cm) and the linear arena (100 × 10 × 30 cm) were made of infrared-transmitting acrylic to allow unobtrusive behavioral monitoring. They were connected by a one-way tunnel (20 × 3 × 3 cm) for entering the arena and a 20 × 5 × 30 cm safe zone with a 5 × 5 cm one-way

door for returning to the nest. Because it was not directly under the monitor, the safe zone was darker than the arena.

Mice were identified using implanted RFID tags, which were detected by an RFID reader positioned around the tunnel. Only one mouse was allowed to enter the arena at a time. Specifically, when all mice were in the nest, the door between the nest and the tunnel was open, while the door between the tunnel and the arena remained closed. When a single mouse entered the tunnel, as detected by the RFID system, the door to the nest closed, and the door to the arena opened, allowing the mouse to enter the arena. Mice received rewards at the end of the arena in the form of water or 10% sucrose. Licking time and reward volume were recorded for each trial.

To track mouse position in real time, an OpenMV camera with a 90° field-of-view lens was mounted on the ground, 110 cm beneath the arena. The mouse position was used to control the tunnel doors and to trigger stimulus presentation when the mouse entered the arena. A second camera (LBAS-U350-74M) with a lens (FA0615A) was also placed on the ground to record animal behavior at 30 frames per second.

Visual stimulation

Looming stimuli were presented on a 55-in. monitor (121 × 68 cm) suspended 32 cm above the arena. Visual stimuli were generated using PsychoPy in Python and aligned to the mouse's real-time location. The stimulus consisted of a black disc that expanded ten times on a gray background (~65 cd/cm^2). On each expansion, the disc grew from 0° to 20° of visual angle at 40°/s, followed by a stationary phase lasting 0.3 s. The inter-stimulus interval was randomly varied between 1 and 2 min. Two stimulus contrasts (20% and 99%) were displayed by adjusting the luminance of the disc.

Economic modulation of innate decision-making

All mice were habituated to the behavioral platform for 2 days before the looming experiment. During both habituation and testing, three reward conditions were used: no reward, water, or 10% sucrose. Mice were not water-deprived in any of the groups. On the first day, five mice from the same home cage were placed in the nest for 30 min with all doors closed. Each mouse was then placed individually in the nest and allowed to explore the arena for 10 min under normal door operation; if a mouse entered the arena fewer than two times, the exploration period was extended until at least two arena visits were completed. Subsequently, all five mice were returned to the nest with all doors open and allowed to freely explore the arena for 2 hr to ensure that each mouse learned the reward location at the end of the linear arena. On the second day, each mouse was placed individually in the nest and given an additional 1 hr of exploration under normal door operation to further acclimate to the environment. The looming experiment was conducted the following day. An overhead looming stimulus of either low (20%) or high (99%) contrast was triggered when the mouse entered the trigger zone, defined as the region within 20 cm of the reward port. For each mouse, both the looming contrast and reward type remained constant across trials. In total, we collected and analyzed behavioral data from 590 trials across 62 mice.

To control for inter-individual variation in decision-making, we compared the same animal's behavior under reward and no-reward conditions. Two groups of mice were used in this experiment. In the first group (n = 4), mice were first tested under the no-reward condition, followed by the reward condition. In the second group (n = 5), the order was reversed. For the reward condition, mice were water-deprived 1 day before exploration, and water was provided via the reward port. In the no-reward condition, mice were not water-deprived, and the reward port was removed. Before the looming experiment, mice were acclimated to the linear arena for 2 days as described above. On the third day, a looming stimulus with 20% contrast was displayed for five trials. In total, behavioral data from 84 trials across 9 mice were recorded and analyzed.

Social modulation of innate decision-making

To investigate the impact of social hierarchy on decision-making, we first determined the social rank of each mouse pair using the tube test (***Wang et al., 2011***; ***Lindzey et al., 1961***), in which dominance is determined by the ability of one individual to force its opponent to retreat from a narrow tube. Mice were co-housed with a glass tube (3 cm diameter, 10 cm long) for 1 week, then trained to traverse a 30-cm tube 10 times per day for two consecutive days. On the third day, each pair was tested for up

to six trials; if one mouse achieved four consecutive wins, it was designated the dominant individual; otherwise, the pair (one out of six pairs) was excluded from further experiments.

Before the looming experiment, mice were water-deprived and allowed to explore the linear arena for 2 hr per day over 3 days, during which water rewards were delivered at the end of the arena. Over the following 2 days, the looming experiment was conducted with a stimulus contrast of 99% for 2 hr per day. After the looming experiment, mice continued exploring the arena for an additional 2 days, after which their social rank was reassessed with the tube test. All remaining pairs maintained a stable rank order. In total, behavioral data from 100 trials across 10 mice were recorded and analyzed.

To assess whether the tube test itself influenced defensive decision-making, additional looming experiments were conducted on four mouse pairs before and after the tube test. Specifically, the first looming experiment was conducted before the tube test (***Figure 4—figure supplement 2A***). Behavioral data from 80 trials across 8 mice were recorded and analyzed.

Behavioral quantification

Animal behaviors were quantified in three steps. First, two key points—the nose and tail base—were labeled and tracked in the recorded videos using DeepLabCut (***Mathis et al., 2018***). Tracked points with likelihood scores below 0.6 were excluded and replaced using linear interpolation. Locomotion speed was calculated for each frame and smoothed using a 0.3-s moving average window. Unless otherwise specified, tail base speed was used for subsequent analyses. Second, individual 30-s trials were extracted, each consisting of 10 s before, 8 s during, and 12 s after the looming stimulus.

Third, we defined 19 behavioral features related to locomotion speed, distance, and state transitions. Eleven features were related to speed and distance: (1) peak speed toward the reward port before stimulus onset; (2–4) maximum, mean, and coefficient of variation of speed after stimulus onset; (5) latency to peak speed; (6) hiding latency, defined as the time between stimulus onset and arrival at the safe zone (set to 20 s if the mouse did not reach the safe zone by the end of the trial); (7) escape distance, defined as the displacement from stimulus onset to offset; (8) distance to the nest at the end of the trial; (9) total distance traveled at speeds greater than 90% of the peak speed; (10) duration of movement at speeds greater than 90% of the peak speed; and (11) duration of time with both key points moving slower than 1 cm/s. Eight features were related to state transitions: (12) latency to flee, defined as the time from stimulus onset to the first escape episode, where an escape state was defined as movement exceeding 10 cm at a speed exceeding 10 cm/s; (13–15) average speed, distance traveled, and acceleration during the fastest escape episode; (16) latency to the fastest escape episode; (17) latency to the first stationary episode, where a stationary state was defined as both key points moving at less than 1 cm/s for more than 0.3 s; (18) total stationary duration and (19) longest stationary duration.

Finally, these features were fed into a random forest model with a maximum depth of 5 to classify behaviors. For trials in which neither escape nor stationary states were identified, latencies (features 12, 16, and 17) were set to 20 s, distance (14) to 0 cm, speed (13) to 0 cm/s, acceleration (15) to 0 cm/s^2, and duration (18, 19) to 0 s. The model was trained on 238 trials and tested on 102 trials, achieving an accuracy of 0.95 on the test set. Using this classifier, behavioral decisions in 3862 trials across 140 mice were categorized into four types: direct escape, escape after assessment, freezing, and no response (***Figure 1—figure supplement 1***). A decision score was calculated for each condition as $S = 3p_e + 2p_{ae} + p_f$, where p_e, p_{ae}, and p_f denote the proportions of direct escape, escape after assessment, and freezing, respectively. To quantify how quickly animals recovered from a fear state, we measured recovery time. For escape trials, recovery time was defined as the hiding duration, measured from entry into the safe zone to re-entry into the arena. For freezing trials, recovery time was defined as the interval between the onset of the first freezing episode and the termination of the last freezing episode.

To quantify the influence of reward, the reward zone was defined as a region within 10 cm of the reward port, and the duration in the reward zone was defined as the time spent within this zone during the 20 s following stimulus onset. Vigilance was assessed using latency to flee, foraging interval (time between two consecutive entries into the trigger zone), and foraging speed (average speed while approaching the trigger zone before stimulus onset).

To segment the trials into two phases, we performed principal component analysis on a feature matrix containing decision score, escape distance, duration in the reward zone, peak escape speed,

and latency to flee across the first 10 trials. We extracted the first principal component (***Figure 2—figure supplement 1C, D***), which captured the majority of the variance, and used its learning curve to detect transitions in behavior. Change points in the learning curve were detected using the ruptures method (***Gallistel et al., 2004***; ***Truong et al., 2020***).

Behavioral modeling

Parameters in the drift-diffusion leaky integrator model were estimated in two steps by minimizing a loss function using a grid search. In the first step, we fit our model to behavioral data from the no-reward condition, setting $r = 0$ and $\beta = 1$ for the low-threat condition, and estimated α, δ, x_{thr}, and β for the high-threat condition. In the second step, we estimated β and r for the water and sucrose conditions under both threat conditions. The loss function combines fitting errors in the distribution of behavioral decisions ($\mathcal{L}_{\text{dec}}$), the median latency to flee ($\mathcal{L}_{\text{med}}$), and the variability of latency ($\mathcal{L}_{\text{sd}}$):

$$\mathcal{L} = 100\mathcal{L}_{\text{dec}} + 2\mathcal{L}_{\text{med}} + \mathcal{L}_{\text{sd}}. \tag{3}$$

The decision-distribution mismatch is quantified using a mean cosine distance:

$$\mathcal{L}_{\text{dec}} = \frac{1}{C}\sum_{c=1}^{C}\left(1 - \frac{\mathbf{d}_c \cdot \hat{\mathbf{d}}_c}{\|\mathbf{d}_c\|\|\hat{\mathbf{d}}_c\|}\right), \tag{4}$$

where $\mathbf{d}_c$ and $\hat{\mathbf{d}}_c$ denote the observed and model-predicted decision distributions for threat intensity c, and $C = 2$ is the number of threat conditions.

The median-latency loss is defined as

$$\mathcal{L}_{\text{med}} = \frac{1}{C}\sum_{c=1}^{C}\frac{\left|\hat{L}_c^{\text{med}} - L_c^{\text{med}}\right|}{\hat{L}_c^{\text{med}} + L_c^{\text{med}}}, \tag{5}$$

and the latency-variability loss is

$$\mathcal{L}_{\text{sd}} = \frac{1}{C}\sum_{c=1}^{C}\frac{\left|\hat{L}_c^{\text{sd}} - L_c^{\text{sd}}\right|}{\hat{L}_c^{\text{sd}} + L_c^{\text{sd}}}. \tag{6}$$

For the final fitted model (***Equation 1***), $\alpha = 1.78$ and $\delta = 5.6$. Under low-threat conditions, $\beta = 1$ for all reward conditions; under high-threat conditions, $\beta = 1.44, 1.8, 2.55$ for no reward, water, and sucrose, respectively. The reward values were $r = 0, 0.08, 0.25$ for no reward, water, and sucrose, respectively, under both threat conditions. In ***Equation 2***, the decision threshold was $x_{\text{thr}} = 0.71$.

To further understand how threat and reward shape decisions, we analyzed a deterministic simplification of the model:

$$\frac{\mathrm{d}x}{\mathrm{d}t} = -\alpha x(t) + nt - p, \tag{7}$$

where $p > 0$ denotes the perceived reward value and $n > 0$ determines the rate at which threat-driven input increases over time.

With the initial condition $x(0) = 0$, the solution is

$$x(t) = \frac{n}{\alpha}t + \left(\frac{p}{\alpha} + \frac{n}{\alpha^2}\right)\left(e^{-\alpha t} - 1\right). \tag{8}$$

This solution reveals a competition between two components. First, a linear term driven by threat accumulation promotes escape over time. Second, an exponentially decaying component reflects the combined influence of reward and threat.

Quantification and statistical analysis

No statistical method was used to predetermine sample size. The Shapiro–Wilk test was applied to assess the normality of data distributions. For comparisons between two groups, a two-sample t-test or paired t-test was used for normally distributed data; otherwise, the Mann–Whitney U test or Wilcoxon signed-rank test was applied. For multi-group comparisons, one- or two-way ANOVA was

used when data were normally distributed, followed by Tukey's post hoc test. For non-parametric multi-group comparisons, the Kruskal–Wallis test (for one factor) or the Scheirer–Ray–Hare test (for two factors) was applied, followed by Dunn's post hoc test with Holm correction. The chi-squared test was used to analyze categorical variables, while paired categorical comparisons were assessed using the Stuart–Maxwell test. Detailed statistical information for each experiment is provided in the Results section and the figure legends.

Acknowledgements

We thank Lei Zhang, Xueting Sun, Haojun Sang, Qun Zhang, Bing Zhao, and Zhuofan Li in the CIBR Instrumentation Core for their help in designing and building the linear arena. Ling-yun Li was supported by the Natural Science Foundation of Beijing Municipality (5244028), the National Natural Science Foundation of China (32471071), and the R&D Program of Beijing Municipal Education Commission (1240030201). Ya-tang Li was supported by the National Natural Science Foundation of China (32271060), the Natural Science Foundation of Beijing Municipality (IS23073), and the startup fund from CIBR.

Additional information

Funding

Funder	Grant reference number	Author
Natural Science Foundation of Beijing Municipality	5244028	Ling-yun Li
National Natural Science Foundation of China	32471071	Ling-yun Li
R&D Program of Beijing Municipal Education Commission	1240030201	Ling-yun Li
Natural Science Foundation of Beijing Municipality	IS23073	Ya-tang Li
National Natural Science Foundation of China	32271060	Ya-tang Li

The funders had no role in study design, data collection, and interpretation, or the decision to submit the work for publication.

Author contributions

Zhe Li, Conceptualization, Data curation, Formal analysis, Investigation, Visualization, Methodology; Jiahui Wang, Formal analysis; Yidan Sun, Conceptualization, Methodology; Jialin Li, Methodology; Ling-yun Li, Supervision, Funding acquisition, Writing – review and editing; Ya-tang Li, Conceptualization, Supervision, Funding acquisition, Investigation, Visualization, Methodology, Writing – original draft, Writing – review and editing

Author ORCIDs

Zhe Li https://orcid.org/0000-0003-1050-3683
Ling-yun Li https://orcid.org/0009-0005-3495-2602
Ya-tang Li https://orcid.org/0000-0003-2763-1534

Ethics

All experimental procedures were performed under the animal welfare guidelines and approved by the Institutional Animal Care and Use Committee (IACUC) at the Chinese Institute for Brain Research, Beijing. Animals were handled according to the approved protocol (CIBR-IACUC-046).

Peer review material

Version of Record:

Reviewer #1 (Public review): https://doi.org/10.7554/eLife.107306.5.sa1
Author response https://doi.org/10.7554/eLife.107306.5.sa2

Reviewed preprint v4
Reviewer #1 (Public review): https://doi.org/10.7554/eLife.107306.4.sa1
Author response: https://doi.org/10.7554/eLife.107306.4.sa0
eLife Assessment https://doi.org/10.7554/eLife.107306.4.sa2

Reviewed preprint v3
Reviewer #1 (Public review): https://doi.org/10.7554/eLife.107306.3.sa1
Author response: https://doi.org/10.7554/eLife.107306.3.sa0
eLife Assessment https://doi.org/10.7554/eLife.107306.3.sa2

Reviewed preprint v2
Reviewer #1 (Public review): https://doi.org/10.7554/eLife.107306.2.sa3
Reviewer #2 (Public review): https://doi.org/10.7554/eLife.107306.2.sa2
Reviewer #3 (Public review): https://doi.org/10.7554/eLife.107306.2.sa1
Author response: https://doi.org/10.7554/eLife.107306.2.sa0
eLife Assessment https://doi.org/10.7554/eLife.107306.2.sa4

Reviewed preprint v1
Reviewer #1 (Public review): https://doi.org/10.7554/eLife.107306.1.sa2
Reviewer #2 (Public review): https://doi.org/10.7554/eLife.107306.1.sa1
Reviewer #3 (Public review): https://doi.org/10.7554/eLife.107306.1.sa0
eLife Assessment https://doi.org/10.7554/eLife.107306.1.sa3

Additional files

Supplementary files
MDAR checklist

Data availability
Data and code are publicly available at GitHub (https://github.com/YatangLiLab/li-2025-economic-social-modulation; copy archived at ***Li, 2026a***).

References

Amir A, Lee SC, Headley DB, Herzallah MM, Pare D. 2015. Amygdala signaling during foraging in a hazardous environment. *The Journal of Neuroscience* **35**:12994–13005. DOI: https://doi.org/10.1523/JNEUROSCI.0407-15.2015, PMID: 26400931

Andermann ML, Kerlin AM, Reid RC. 2010. Chronic cellular imaging of mouse visual cortex during operant behavior and passive viewing. *Frontiers in Cellular Neuroscience* **4**:3. DOI: https://doi.org/10.3389/fncel.2010.00003, PMID: 20407583

Anderson DJ, Adolphs R. 2014. A framework for studying emotions across species. *Cell* **157**:187–200. DOI: https://doi.org/10.1016/j.cell.2014.03.003, PMID: 24679535

Barnes CA. 1979. Memory deficits associated with senescence: a neurophysiological and behavioral study in the rat. *Journal of Comparative and Physiological Psychology* **93**:74–104. DOI: https://doi.org/10.1037/h0077579, PMID: 221551

Baruchin LJ, Alleman M, Schröder S. 2023. Reward Modulates visual responses in the superficial superior colliculus of mice. *The Journal of Neuroscience* **43**:8663–8680. DOI: https://doi.org/10.1523/JNEUROSCI.0089-23.2023, PMID: 37879894

Benavidez NL, Bienkowski MS, Zhu M, Garcia LH, Fayzullina M, Gao L, Bowman I, Gou L, Khanjani N, Cotter KR, Korobkova L, Becerra M, Cao C, Song MY, Zhang B, Yamashita S, Tugangui AJ, Zingg B, Rose K, Lo D, et al. 2021. Organization of the inputs and outputs of the mouse superior colliculus. *Nature Communications* **12**:4004. DOI: https://doi.org/10.1038/s41467-021-24241-2, PMID: 34183678

Bravo-Rivera C, Roman-Ortiz C, Brignoni-Perez E, Sotres-Bayon F, Quirk GJ. 2014. Neural structures mediating expression and extinction of platform-mediated avoidance. *The Journal of Neuroscience* **34**:9736–9742. DOI: https://doi.org/10.1523/JNEUROSCI.0191-14.2014, PMID: 25031411

Buck L. 1966. Reaction time as a measure of perceptual vigilance. *Psychological Bulletin* **65**:291–304. DOI: https://doi.org/10.1037/h0023207, PMID: 5325893

Burgess CP, Lak A, Steinmetz NA, Zatka-Haas P, Bai Reddy C, Jacobs EAK, Linden JF, Paton JJ, Ranson A, Schröder S, Soares S, Wells MJ, Wool LE, Harris KD, Carandini M. 2017. High-yield methods for accurate two-alternative visual psychophysics in head-fixed mice. *Cell Reports* **20**:2513–2524. DOI: https://doi.org/10.1016/j.celrep.2017.08.047, PMID: 28877482

Calvin OL, Erickson MT, Walters CJ, Redish AD. 2025. Dorsal hippocampus represents locations to avoid as well as locations to approach during approach-avoidance conflict. *PLOS Biology* **23**:e3002954. DOI: https://doi.org/10.1371/journal.pbio.3002954, PMID: 39808614

Campagner D, Vale R, Tan YL, Iordanidou P, Pavón Arocas O, Claudi F, Stempel AV, Keshavarzi S, Petersen RS, Margrie TW, Branco T. 2023. A cortico-collicular circuit for orienting to shelter during escape. *Nature* **613**:111–119. DOI: https://doi.org/10.1038/s41586-022-05553-9, PMID: 36544025

Caraco T, Martindale S, Pulliam HR. 1980. Avian flocking in the presence of a predator. *Nature* **285**:400–401. DOI: https://doi.org/10.1038/285400a0

Choi JS, Kim JJ. 2010. Amygdala regulates risk of predation in rats foraging in a dynamic fear environment. *PNAS* **107**:21773–21777. DOI: https://doi.org/10.1073/pnas.1010079108

Cohen JY, Haesler S, Vong L, Lowell BB, Uchida N. 2012. Neuron-type-specific signals for reward and punishment in the ventral tegmental area. *Nature* **482**:85–88. DOI: https://doi.org/10.1038/nature10754, PMID: 22258508

Comoli E, Coizet V, Boyes J, Bolam JP, Canteras NS, Quirk RH, Overton PG, Redgrave P. 2003. A direct projection from superior colliculus to substantia nigra for detecting salient visual events. *Nature Neuroscience* **6**:974–980. DOI: https://doi.org/10.1038/nn1113, PMID: 12925855

Comoli E, Das Neves Favaro P, Vautrelle N, Leriche M, Overton PG, Redgrave P. 2012. Segregated anatomical input to sub-regions of the rodent superior colliculus associated with approach and defense. *Frontiers in Neuroanatomy* **6**:9. DOI: https://doi.org/10.3389/fnana.2012.00009, PMID: 22514521

Constantinople CM, Piet AT, Brody CD. 2019. An analysis of decision under risk in rats. *Current Biology* **29**:2066–2074. DOI: https://doi.org/10.1016/j.cub.2019.05.013, PMID: 31155352

Conway PB, Autore L, Muñoz Zamora A, Harel A, Wang Z, Tavallaei AA, Winston SM, Ortega-de San Luis C, O'Leary JD, Brimble MA, Vetere G, Ryan TJ. 2025. Extinction and subsequent updating of innate fear responses to a visual looming stimulus rely on hippocampus-dependent mechanisms. *PLOS Biology* **23**:e3003391. DOI: https://doi.org/10.1371/journal.pbio.3003391, PMID: 40991660

De Franceschi G, Vivattanasarn T, Saleem AB, Solomon SG. 2016. Vision guides selection of freeze or flight defense strategies in mice. *Current Biology* **26**:2150–2154. DOI: https://doi.org/10.1016/j.cub.2016.06.006, PMID: 27498569

Edwards DH, Kravitz EA. 1997. Serotonin, social status and aggression. *Current Opinion in Neurobiology* **7**:812–819. DOI: https://doi.org/10.1016/s0959-4388(97)80140-7, PMID: 9464985

Evans DA, Stempel AV, Vale R, Ruehle S, Lefler Y, Branco T. 2018. A synaptic threshold mechanism for computing escape decisions. *Nature* **558**:590–594. DOI: https://doi.org/10.1038/s41586-018-0244-6, PMID: 29925954

Evans DA, Stempel AV, Vale R, Branco T. 2019. Cognitive control of escape behaviour. *Trends in Cognitive Sciences* **23**:334–348. DOI: https://doi.org/10.1016/j.tics.2019.01.012

Fanselow MS, Lester LS. 1988. A functional behavioristic approach to aversively motivated behavior: predatory imminence as a determinant of the topography of defensive behavior. In: Bolles RC, Beecher MD (Eds). *Evolution and Learning*. Lawrence Erlbaum Associates. p. 185–212.

Fratzl A, Koltchev AM, Vissers N, Tan YL, Marques-Smith A, Stempel AV, Branco T, Hofer SB. 2021. Flexible inhibitory control of visually evoked defensive behavior by the ventral lateral geniculate nucleus. *Neuron* **109**:3810–3822. DOI: https://doi.org/10.1016/j.neuron.2021.09.003, PMID: 34614420

Gallistel CR, Fairhurst S, Balsam P. 2004. The learning curve: Implications of a quantitative analysis. *PNAS* **101**:13124–13131. DOI: https://doi.org/10.1073/pnas.0404965101

Gibson WT, Gonzalez CR, Fernandez C, Ramasamy L, Tabachnik T, Du RR, Felsen PD, Maire MR, Perona P, Anderson DJ. 2015. Behavioral responses to a repetitive visual threat stimulus express a persistent state of defensive arousal in *Drosophila*. *Current Biology* **25**:1401–1415. DOI: https://doi.org/10.1016/j.cub.2015.03.058, PMID: 25981791

Hayden BY, Pearson JM, Platt ML. 2011. Neuronal basis of sequential foraging decisions in a patchy environment. *Nature Neuroscience* **14**:933–939. DOI: https://doi.org/10.1038/nn.2856, PMID: 21642973

Hayden BY. 2018. Economic choice: the foraging perspective. *Current Opinion in Behavioral Sciences* **24**:1–6. DOI: https://doi.org/10.1016/j.cobeha.2017.12.002

Kahneman D, Tversky A. 1979. Prospect theory: an analysis of decision under risk. *Econometrica* **47**:263. DOI: https://doi.org/10.2307/1914185

Kingsbury L, Huang S, Wang J, Gu K, Golshani P, Wu YE, Hong W. 2019. Correlated neural activity and encoding of behavior across brains of socially interacting animals. *Cell* **178**:429–446. DOI: https://doi.org/10.1016/j.cell.2019.05.022, PMID: 31230711

Kleiman M, Bodek S, Eilam D. 2014. Who are the bosses? Group influence on the behavior of voles following owl attack. *Behavioural Processes* **108**:183–190. DOI: https://doi.org/10.1016/j.beproc.2014.10.017, PMID: 25444777

Krasne FB, Shamsian A, Kulkarni R. 1997. Altered excitability of the crayfish lateral giant escape reflex during agonistic encounters. *The Journal of Neuroscience* **17**:709–716. DOI: https://doi.org/10.1523/JNEUROSCI.17-02-00709.1997, PMID: 8987792

Krauzlis RJ, Lovejoy LP, Zénon A. 2013. Superior colliculus and visual spatial attention. *Annual Review of Neuroscience* **36**:165–182. DOI: https://doi.org/10.1146/annurev-neuro-062012-170249, PMID: 23682659
Lenzi SC, Cossell L, Grainger B, Olesen SF, Branco T, Margrie TW. 2022. Threat history controls flexible escape behavior in mice. *Current Biology* **32**:2972–2979. DOI: https://doi.org/10.1016/j.cub.2022.05.022, PMID: 35659863
Li YT, Turan Z, Meister M. 2020. Functional architecture of motion direction in the mouse superior colliculus. *Current Biology* **30**:3304–3315. DOI: https://doi.org/10.1016/j.cub.2020.06.023, PMID: 32649907
Li C, Kühn NK, Alkislar I, Sans-Dublanc A, Zemmouri F, Paesmans S, Calzoni A, Ooms F, Reinhard K, Farrow K. 2023. Pathway-specific inputs to the superior colliculus support flexible responses to visual threat. *Science Advances* **9**:3874. DOI: https://doi.org/10.1126/sciadv.ade3874
Li Y. 2026a. Li-2025-economic-social-modulation. swh:1:rev:46c78748ac34aac2caa2178d7b0fc18738c5319e. Software Heritage. https://archive.softwareheritage.org/swh:1:dir:1abd04b3d736252e80faa7f9cbeed258f4b9c1f9;origin=https://github.com/YatangLiLab/li-2025-economic-social-modulation;visit=swh:1:snp:76fd152a86ace32e2b5c4c7bafeb94e765d84be7;anchor=swh:1:rev:46c78748ac34aac2caa2178d7b0fc18738c5319e
Li L, Gao X, Li Y. 2026b. Rank- and threat-dependent social modulation of innate defensive behaviors. *bioRxiv*. DOI: https://doi.org/10.1101/2025.10.31.685719
Liden WH, Herberholz J. 2008. Behavioral and neural responses of juvenile crayfish to moving shadows. *The Journal of Experimental Biology* **211**:1355–1361. DOI: https://doi.org/10.1242/jeb.010165, PMID: 18424668
Lindzey G, Winston H, Manosevitz M. 1961. Social dominance in inbred mouse strains. *Nature* **191**:474–476. DOI: https://doi.org/10.1038/191474a0, PMID: 13762409
Liu Z, Zhou J, Li Y, Hu F, Lu Y, Ma M, Feng Q, Zhang JE, Wang D, Zeng J, Bao J, Kim JY, Chen ZF, El Mestikawy S, Luo M. 2014. Dorsal raphe neurons signal reward through 5-HT and glutamate. *Neuron* **81**:1360–1374. DOI: https://doi.org/10.1016/j.neuron.2014.02.010, PMID: 24656254
Lorenz KZ. 1950. The comparative method in studying innate behavior patterns. *Symposia of the Society for Experimental Biology* **4**:221–268.
Mathis A, Mamidanna P, Cury KM, Abe T, Murthy VN, Mathis MW, Bethge M. 2018. DeepLabCut: markerless pose estimation of user-defined body parts with deep learning. *Nature Neuroscience* **21**:1281–1289. DOI: https://doi.org/10.1038/s41593-018-0209-y, PMID: 30127430
Mederos S, Blakely P, Vissers N, Clopath C, Hofer SB. 2025. Overwriting an instinct: Visual cortex instructs learning to suppress fear responses. *Science* **387**:682–688. DOI: https://doi.org/10.1126/science.adr2247, PMID: 39913581
Meister M. 2022. Learning, fast and slow. *Current Opinion in Neurobiology* **75**:102555. DOI: https://doi.org/10.1016/j.conb.2022.102555, PMID: 35617751
Miyazaki K, Miyazaki KW, Doya K. 2011. Activation of dorsal raphe serotonin neurons underlies waiting for delayed rewards. *The Journal of Neuroscience* **31**:469–479. DOI: https://doi.org/10.1523/JNEUROSCI.3714-10.2011, PMID: 21228157
Mooney RD, Huang X, Shi MY, Bennett-Clarke CA, Rhoades RW. 1996. Serotonin modulates retinotectal and corticotectal convergence in the superior colliculus. *Progress in Brain Research* **112**:57–69. DOI: https://doi.org/10.1016/s0079-6123(08)63320-8, PMID: 8979820
Morris R. 1984. Developments of a water-maze procedure for studying spatial learning in the rat. *Journal of Neuroscience Methods* **11**:47–60. DOI: https://doi.org/10.1016/0165-0270(84)90007-4, PMID: 6471907
Moscarello JM, LeDoux JE. 2013. Active avoidance learning requires prefrontal suppression of amygdala-mediated defensive reactions. *The Journal of Neuroscience* **33**:3815–3823. DOI: https://doi.org/10.1523/JNEUROSCI.2596-12.2013, PMID: 23447593
Mowrer OH, Lamoreaux RR. 1946. Fear as an intervening variable in avoidance conditioning. *Journal of Comparative Psychology* **39**:29–50. DOI: https://doi.org/10.1037/h0060150, PMID: 21018303
Raleigh MJ, McGuire MT, Brammer GL, Pollack DB, Yuwiler A. 1991. Serotonergic mechanisms promote dominance acquisition in adult male vervet monkeys. *Brain Research* **559**:181–190. DOI: https://doi.org/10.1016/0006-8993(91)90001-c, PMID: 1794096
Rangel A, Camerer C, Montague PR. 2008. A framework for studying the neurobiology of value-based decision making. *Nature Reviews. Neuroscience* **9**:545–556. DOI: https://doi.org/10.1038/nrn2357, PMID: 18545266
Ratcliff R. 1978. A theory of memory retrieval. *Psychological Review* **85**:59–108. DOI: https://doi.org/10.1037/0033-295X.85.2.59
Rosenberg M, Zhang T, Perona P, Meister M. 2021. Mice in a labyrinth show rapid learning, sudden insight, and efficient exploration. *eLife* **10**:e66175. DOI: https://doi.org/10.7554/eLife.66175, PMID: 34196271
Salay LD, Huberman AD. 2021. Divergent outputs of the ventral lateral geniculate nucleus mediate visually evoked defensive behaviors. *Cell Reports* **37**:109792. DOI: https://doi.org/10.1016/j.celrep.2021.109792, PMID: 34610302
Schultz W, Apicella P, Scarnati E, Ljungberg T. 1992. Neuronal activity in monkey ventral striatum related to the expectation of reward. *The Journal of Neuroscience* **12**:4595–4610. DOI: https://doi.org/10.1523/JNEUROSCI.12-12-04595.1992, PMID: 1464759
Schultz W. 1998. Predictive reward signal of dopamine neurons. *Journal of Neurophysiology* **80**:1–27. DOI: https://doi.org/10.1152/jn.1998.80.1.1, PMID: 9658025
Shang C, Liu Z, Chen Z, Shi Y, Wang Q, Liu S, Li D, Cao P. 2015. A parvalbumin-positive excitatory visual pathway to trigger fear responses in mice. *Science* **348**:1472–1477. DOI: https://doi.org/10.1126/science.aaa8694, PMID: 26113723

Shang C, Chen Z, Liu A, Li Y, Zhang J, Qu B, Yan F, Zhang Y, Liu W, Liu Z, Guo X, Li D, Wang Y, Cao P. 2018. Divergent midbrain circuits orchestrate escape and freezing responses to looming stimuli in mice. *Nature Communications* **9**:1232. DOI: https://doi.org/10.1038/s41467-018-03580-7, PMID: 29581428

Small WS. 1901. Experimental study of the mental processes of the rat. II. *The American Journal of Psychology* **12**:206. DOI: https://doi.org/10.2307/1412534

Steiner AP, Redish AD. 2014. Behavioral and neurophysiological correlates of regret in rat decision-making on a neuroeconomic task. *Nature Neuroscience* **17**:995–1002. DOI: https://doi.org/10.1038/nn.3740, PMID: 24908102

Steinmetz NA, Zatka-Haas P, Carandini M, Harris KD. 2019. Distributed coding of choice, action and engagement across the mouse brain. *Nature* **576**:266–273. DOI: https://doi.org/10.1038/s41586-019-1787-x, PMID: 31776518

Tammero LF, Dickinson MH. 2002. Collision-avoidance and landing responses are mediated by separate pathways in the fruit fly, *Drosophila melanogaster*. *The Journal of Experimental Biology* **205**:2785–2798. DOI: https://doi.org/10.1242/jeb.205.18.2785, PMID: 12177144

Tremblay L, Schultz W. 2000. Reward-related neuronal activity during go-nogo task performance in primate orbitofrontal cortex. *Journal of Neurophysiology* **83**:1864–1876. DOI: https://doi.org/10.1152/jn.2000.83.4.1864, PMID: 10758098

Truong C, Oudre L, Vayatis N. 2020. Selective review of offline change point detection methods. *Signal Processing* **167**:107299. DOI: https://doi.org/10.1016/j.sigpro.2019.107299

Vale R, Evans DA, Branco T. 2017. Rapid Spatial learning controls instinctive defensive behavior in mice. *Current Biology* **27**:1342–1349. DOI: https://doi.org/10.1016/j.cub.2017.03.031, PMID: 28416117

Wagner MJ, Kim TH, Savall J, Schnitzer MJ, Luo L. 2017. Cerebellar granule cells encode the expectation of reward. *Nature* **544**:96–100. DOI: https://doi.org/10.1038/nature21726, PMID: 28321129

Wallace DJ, Greenberg DS, Sawinski J, Rulla S, Notaro G, Kerr JND. 2013. Rats maintain an overhead binocular field at the expense of constant fusion. *Nature* **498**:65–69. DOI: https://doi.org/10.1038/nature12153, PMID: 23708965

Wang F, Zhu J, Zhu H, Zhang Q, Lin Z, Hu H. 2011. Bidirectional control of social hierarchy by synaptic efficacy in medial prefrontal cortex. *Science* **334**:693–697. DOI: https://doi.org/10.1126/science.1209951, PMID: 21960531

Wei P, Liu N, Zhang Z, Liu X, Tang Y, He X, Wu B, Zhou Z, Liu Y, Li J, Zhang Y, Zhou X, Xu L, Chen L, Bi G, Hu X, Xu F, Wang L. 2015. Processing of visually evoked innate fear by a non-canonical thalamic pathway. *Nature Communications* **6**:6756. DOI: https://doi.org/10.1038/ncomms7756, PMID: 25854147

Woolrych A, Vautrelle N, Reynolds JNJ, Parr-Brownlie LC. 2021. Throwing open the doors of perception: The role of dopamine in visual processing. *The European Journal of Neuroscience* **54**:6135–6146. DOI: https://doi.org/10.1111/ejn.15408, PMID: 34340265

Yang X, Liu Q, Zhong J, Song R, Zhang L, Wang L. 2020. A simple threat-detection strategy in mice. *BMC Biology* **18**:93. DOI: https://doi.org/10.1186/s12915-020-00825-0, PMID: 32727449

Ydenberg RC, Dill LM. 1986. The economics of fleeing from predators. *Advances in the Study of Behavior* **16**:229–249. DOI: https://doi.org/10.1016/S0065-3454(08)60192-8

Yeh SR, Musolf BE, Edwards DH. 1997. Neuronal adaptations to changes in the social dominance status of crayfish. *The Journal of Neuroscience* **17**:697–708. DOI: https://doi.org/10.1523/JNEUROSCI.17-02-00697.1997, PMID: 8987791

Yilmaz M, Meister M. 2013. Rapid innate defensive responses of mice to looming visual stimuli. *Current Biology* **23**:2011–2015. DOI: https://doi.org/10.1016/j.cub.2013.08.015, PMID: 24120636

Zhong J, Liu Q, Yang X, Su J, Li X, Luo M, Wang L. 2023. Mice learn from the predator-attack experience to accelerate flight behavior via optimizing the strategy of environment exploration. *Biochemical and Biophysical Research Communications* **665**:26–34. DOI: https://doi.org/10.1016/j.bbrc.2023.04.060, PMID: 37148743

Zhou Z, Liu X, Chen S, Zhang Z, Liu Y, Montardy Q, Tang Y, Wei P, Liu N, Li L, Song R, Lai J, He X, Chen C, Bi G, Feng G, Xu F, Wang L. 2019. A VTA GABAergic neural circuit mediates visually evoked innate defensive responses. *Neuron* **103**:473–488. DOI: https://doi.org/10.1016/j.neuron.2019.05.027, PMID: 31202540